



Effects of vacuum and calcination temperature on the structure, texture, reactivity, and selectivity of alumina: Experimental and DFT studies

Hossein A. Dabbagh*, Keivan Taban, Mehdi Zamani

Catalysis Research Laboratory, Department of Chemistry, Isfahan University of Technology, Isfahan 841548311, Iran

ARTICLE INFO

Article history:

Received 8 December 2009
Received in revised form 12 April 2010
Accepted 13 April 2010
Available online 20 April 2010

Keywords:

Alumina
Morphology
Vacuum
Syn/anti-elimination
SEM
DFT

ABSTRACT

The effects of vacuum and/or calcination temperature on the structure and texture of alumina were investigated using XRD, SEM, BET, DTG and FT-IR. Elucidation of the observed reactivity and selectivity over the catalyst was carried out via elimination reaction of secondary (2-octanol) and tertiary (1,2-diphenyl-2-propanol, DPP) alcohols. The mechanism of (R)-, (S)-2-octanol and (R)-, (S)-DPP dehydration over (1 0 0) and (1 1 0) surfaces of alumina was modeled using density functional theory (DFT).

© 2010 Elsevier B.V. All rights reserved.

1. Introduction

Alumina compounds are currently used as industrial catalysts, catalyst supports, adsorbents, and ion exchangers because of their thermal, chemical, and mechanical stability [1]. They are generally produced industrially by precipitation, drying, and calcination of aluminum oxy-hydroxides. The catalytic properties of alumina largely depend on their crystalline structure and texture. Therefore, great efforts have been devoted to master these physicochemical properties. Among the synthesis methods that can be used for preparing alumina, the sol–gel method provides an attractive and convenient route, one of its advantages being accurate control over such structural and textural properties as high specific surface area, homogeneous pore size distribution, and high purity. Despite these advantages, application of the method to prepare materials of catalytic interest is not yet as mature as it is in preparing glasses and ceramics [2]. Amini and Mirzaee [3] used various aluminum alkoxide precursors for the preparation of boehmite by hydrothermal assisted sol–gel processing. They reported crystallized boehmite prepared from aluminum isobutoxide or aluminum isopropoxide by hydrothermal hydrolysis at 150 °C. Park et al. [4] reported the preparation of aluminum oxide nanoparticles by the hydrolysis of aluminum isopropoxide followed by calcinations, in the presence of surface stabilizing agents.

The boehmite was obtained in the absence of surfactant. At 600, 1000 and 1200 °C, the predominant oxides are γ -, θ - and α -Al₂O₃, respectively. Le Bihan et al. [5] examined the introduction of chelating agents such as butan-1,3-diol or acetylacetone in the aluminum isopropoxide solution. A decrease in the crystallinity of alumina was observed when the added amount of complexing agent was increased. Kim [6] prepared boehmite by using the hydrolysis of aluminum isopropoxide in a dilute solution of isopropyl alcohol followed by the addition of ammonium hydroxide. According to his report the amorphous alumina was transformed to a crystalline when calcination temperature increased to 500 °C. Between 500 and 900 °C, crystalline alumina was converted to δ -Al₂O₃. The phase conversions and morphological changes of alumina aerogels during the heat treatment were investigated by Keysar et al. [7]. The phase conversions in the range 20–1300 °C were as following: boehmite/pseudoboehmite \rightarrow η -Al₂O₃ \rightarrow θ -Al₂O₃ \rightarrow α -Al₂O₃. Furthermore, several authors have investigated the texture of alumina materials [8–18]. Unfortunately, most of their works were restricted to the synthesis and morphology of aluminas and a detailed understanding of their catalytic properties is still lacking. Surprisingly, there was no reported method for the preparation of alumina under vacuum.

Dehydration of alcohols to alkenes over alumina dates back a nearly century ago [19]. During this period large numbers of publications have addressed the mechanism of these reactions and physicochemical properties of alumina [20–27]. The surface and interior structure of metal oxides are complex and remains to be defined. Understanding the structure of aluminum oxide and the

* Corresponding author. Tel.: +98 311 3913257; fax: +98 311 3912350.
E-mail address: dabbagh@cc.iut.ac.ir (H.A. Dabbagh).

way atoms arrange in space in these oxides is the cornerstone of investigations for the past century. The widely accepted model, proposed by Peri [23] assumes a random configuration of hydroxyl groups after dehydration leaving adjoining residual oxide ions, oxide vacancies and exposed aluminum ions. Recently, we depicted γ - Al_2O_3 formation from aluminum isopropoxide as a polymerization process and initiated a detail analysis of elimination reaction of secondary and tertiary alcohols over pure and modified γ - Al_2O_3 [26,27]. The major difference in aluminum oxide polymer is that the bonds have more ionic character. Loss of hydroxyl groups from polymer chain would increase the cross-links producing larger particle size. Further, it was concluded that the dehydration of alcohols over metal oxides depends on not only the steric interaction of the intermediate and/or transition state but is also strongly dependent on the preparation conditions of the catalyst and reaction conditions. Dabbagh and Yalfani investigated the effect morphology of alumina and mixed alumina–thorium oxide on reactivity and selectivity of alcohol dehydration [27].

A defect spinel-like structure is commonly accepted for γ - Al_2O_3 [28]. Spinel has 24 cations and 32 anions in the cubic unit cell. In the ideal spinel structure the aluminum atoms occupy 10% of the tetrahedral sites and 46.7% of the octahedral sites formed by the cubic close-packed array of oxygen atoms. However, to satisfy the Al_2O_3 stoichiometry, some Al vacancies must be introduced. This is the origin of the historical formula for the conventional cubic cell $\text{Al}_{21+1/3\Box+2/3}\text{O}_{32}$, where \Box denotes a vacancy at the spinel sites.

Recently, theoretical calculations have developed new models of γ - Al_2O_3 [29–45]. Ionescu et al. [29] and Maresca et al. [30] provide an exhaustive study about structural and electronic properties of γ - Al_2O_3 ideal spinel structure. The distribution of vacancies into this structure has been the subject of great controversy [31]. Some studies indicate that the vacancies are at tetrahedral sites, others at octahedral, and others show different proportions of tetrahedral and octahedral vacancies. The correlation between the positions of the cation vacancies and the energies of the possible structures was examined by Gutierrez et al. [31] and Taniike et al. [32]. They concluded that an octahedral vacancy was more stable than a tetrahedral vacancy.

Sohlberg et al. [33–36] supported the presence of various amounts of hydrogen within the bulk structure of spinel γ - Al_2O_3 . While Wolverton and Hass [37] indicated that hydrogen spinel is thermodynamically unstable with respect to decomposition into an anhydrous defect spinel plus boehmite. Digne et al. [38–41] reported a complete non-spinel structure based on molecular dynamic simulations and DFT calculations of the dehydration of boehmite. Nelson et al. performed DFT and simulated XRD calculations for identification of three different spinel-related γ - Al_2O_3 structures (fully and partly hydrogenated structures and defect spinel) versus non-spinel models [42,43]. They have concluded that the spinel-related structure model is better than the non-spinel model for describing the structure of the bulk γ - Al_2O_3 . This idea immediately was criticized by Paglia et al. [44]. They showed that a non-spinel structure matches data from neutron diffraction experiments [45]. Recently, a single crystal X-ray diffraction study of γ - Al_2O_3 was reported by Smrcok et al. [46]. Refined occupancy parameters indicate that, in addition to the ideal spinel positions, approximately 6% of Al ions also occupy non-spinel positions. Such a cation distribution is in accord with the results of Paglia et al. [45].

Unlike many reported studies that concentrate on hydrothermal process adjustments, the present work focuses on the calcination process and the effects of temperature and vacuum on subsequent properties (structure, texture, reactivity and selectivity) of the synthesized alumina. Finally, the molecular adsorption of alcohols (2-octanol and DPP) stereo isomers with the key conformers

was investigated over the (1 0 0) and (1 1 0) surface of defect spinel γ - Al_2O_3 using DFT/BLYP (Becke–Lee–Yang–Parr) [47,48] level of calculation. These results and experimental finding were utilized for detailed understanding of the mechanism of elimination of these alcohols over γ - Al_2O_3 .

2-Octanol and DPP were selected for the following reasons. First, the dehydration of secondary and tertiary alcohols was investigated in one run under identical conditions. Second, high concentration of 2-octanol was used as solvent to prevent isomerization. Third, DPP has the potential for producing carbocation intermediate (stabilizes by resonance and hyperconjugation). This helps predict the mechanism of dehydration.

2. Experimental

2.1. Catalyst preparation

Aluminum isopropoxide was hydrolyzed in deionized water and stirred for 30 min at room temperature until homogenous slurry was obtained. The resulting suspension was dried at 120 °C for 2 days. The powder was then milled and the particle size was determined (mesh size = 100–200). Boehmite was exposed to calcination temperatures and pressures. Samples were calcined at 120 °C (BCT₁₂₀NV), 250 °C (BCT₂₅₀NV), and 350 °C (BCT₃₅₀NV) under atmospheric pressure (NV, no vacuum) for 24 h; at 250 °C (BCT₂₅₀LV) and 350 °C (BCT₃₅₀LV) under 0.01 bar for 24 h; and at 600 °C (BCT₆₀₀NV) under the atmospheric pressure (BCT₆₀₀LV) under 0.01 bar (LV, low vacuum), and (BCT₆₀₀HV) under 1×10^{-6} bar (HV, high vacuum) for 6 h.

2.2. Catalyst characterization

X-ray diffraction (XRD) patterns were collected on powder diffractometer model Philips Xpert MPD using a Cu K α radiation source ($\lambda = 1.51418 \text{ \AA}$). Scanning electron microscopy (SEM) experiments were performed using a Philips XLC electron microscope. Samples were vapor-deposited with gold before analysis. Infrared (IR) spectra were recorded on a Jasco-FT-IR-680 plus apparatus using KBr transparent discs. TGA and DTG curves were analyzed on a LINAIS-L70/2171 apparatus. The single point BET analysis was performed by nitrogen physisorption at 298 K after outgassing at 300 °C using an AFAP 2000.

2.3. Catalytic activity and selectivity measurements

1,2-Diphenyl-2-propanol (DPP) was prepared according to the Grignard method reported earlier [26]. Elimination reactions of 2-octanol and DPP were carried out over the catalysts (BCT₂₅₀NV, BCT₂₅₀LV, BCT₃₅₀NV, BCT₃₅₀LV, BCT₆₀₀NV, BCT₆₀₀LV and BCT₆₀₀HV) at the reaction temperature 280 °C (the reaction temperature over BCT₂₅₀ catalysts was 250 °C). The catalytic reactions were performed in a vertical plug flow reactor made of Pyrex glass and fitted with a thermal well extended to the center of the catalyst bed. About 20–30 cm³ of the reactor volume above the catalyst bed contained Pyrex glass beads to serve as preheater. A 4% solution of DPP in 2-octanol was exposed to the catalyst at a flow rate of 18 cm³/h. Liquid products were collected at room temperature at increasing time intervals. Alcohol conversion and product distribution were monitored using the Agilent 6890N gas chromatograph equipped with a capillary HP-5 column. The column properties were: 30 m long, 0.32 mm in inner diameter, and 0.25 μm film thick. The column stationary phase was (5% phenyl)-methyl polysiloxane. The products were identified using the Fisons 8060 GC-MASS instrument equipped with a 30 m HP-5 capillary column.

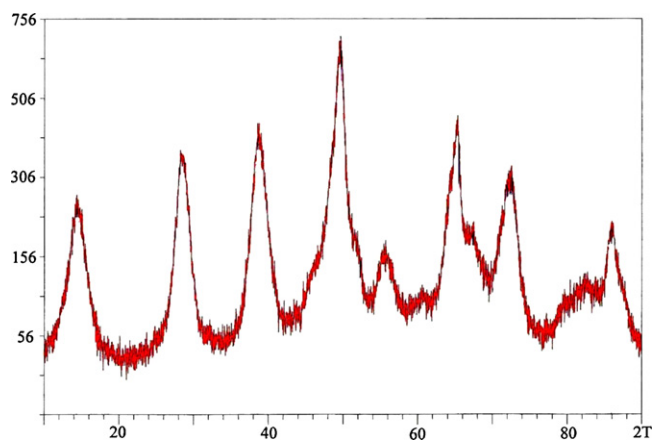


Fig. 1. XRD pattern of boehmite dried at 120 °C (BCT₁₂₀NV) under one atmosphere.

2.4. Computational details

Potential energy scan (PES) of alcohols in order to search the conformers with minimum energy was performed at HF/6-31G** level of calculation using the GAUSSIAN 03 program [49]. The final DFT calculations were performed on the more stable conformers using the DMOL³ program [50,51]. The double numerical plus polarization function (DNP) [50,51] and BLYP [47,48] generalized gradient approximation were used in all calculations. It should be mentioned that the DNP basis set includes a double-zeta quality basis set that a p-type polarization function added to hydrogen and d-type polarization functions added to heavier atoms, and is equivalent to 6-31G** Gaussian basis sets [52]. Each basic function was restricted to a cutoff radius of 4.5 Å. Effective core potentials (ECP) were used to treat the core electrons and a k-point set separation of 0.07 Å⁻¹. The tolerance of the energy change was set to medium (2.0 e⁻⁵ Ha) for all calculations.

The (1 0 0) and (1 1 0) surface orientations from defect spinel γ-Al₂O₃, based on the earlier Ionescu et al. model [29,53], were cleaved. The effects of the surface defects previously reported in Ref. [53]. We imposed a vacuum of 15 Å between slabs in the direction of the crystal lattice, perpendicular to the surface plane, and periodically repeated the unit cell through space. Also, we selected four layers of atoms (Al₆₄O₉₆ for (1 0 0) and Al₄₈O₆₄ for (1 1 0) surfaces) while, the two bottom layers of the slab were constrained. The main specific feature of these surfaces is the asymmetric property. This feature stems from the holes and vacancies of the defect γ-Al₂O₃ bulk structure.

There are several literature reports describing the molecular adsorption of alcohols over the hydroxylated γ-Al₂O₃ surfaces [34,54]. This study focuses on the molecular adsorption of the

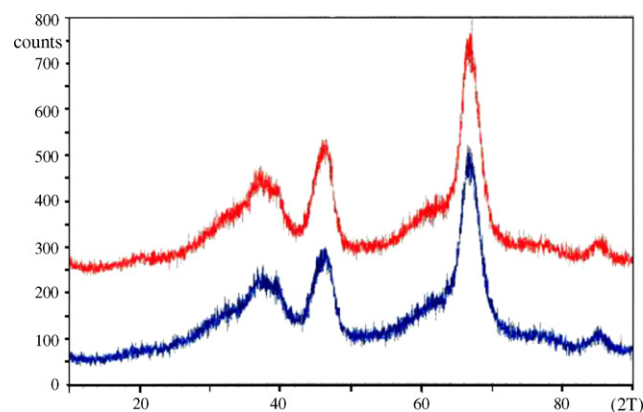


Fig. 3. XRD patterns for the boehmite after calcination at 350 °C. BCT₃₅₀NV (top) and BCT₃₅₀LV (bottom).

title molecules over the dehydroxylated surface. Most experimental results of alcohol dehydration are reported over the catalysts calcined at 600 °C. This catalyst shows small number of hydroxyl over the surface. This model surface can play an important role at higher temperatures.

The adsorption energy (ΔE_{ads}) of alcohol was calculated as:

$$\Delta E_{\text{ads}} = E_{(\text{adsorbed alcohol on surface})} - E_{(\text{alcohol})} - E_{(\text{surface})}$$

where $E_{(\text{adsorbed alcohol on surface})}$ refers to the energy of the system which is formed by an adsorbed alcohol and the surface. $E_{(\text{alcohol})}$ and $E_{(\text{surface})}$ refer to the energy of an isolated alcohol and the bare surface.

To determine the activation energy for a specific reaction pathway, a transition state was identified by the complete linear synchronous transit (LST) and the quadratic synchronous transit (QST) methods.

3. Results and discussion

3.1. XRD measurement

We assessed the XRD spectra in order to realize which kind of transition alumina had formed. In addition, according to peak heights and peak widths, we presented some qualitative explanation of crystallinity and particle size. The XRD pattern of the dried powder (BCT₁₂₀NV) prepared under the atmospheric pressure at 120 °C (Fig. 1) showed reasonable compatibility with the boehmite spectrum reported in the literature [55–58]. Evaluation of XRD diagrams of catalysts prepared at 250 °C (Fig. 2) predicted that γ-Al₂O₃ phase would not be completed, but that the existing phase (of the catalyst prepared under vacuum, BCT₂₅₀LV) would

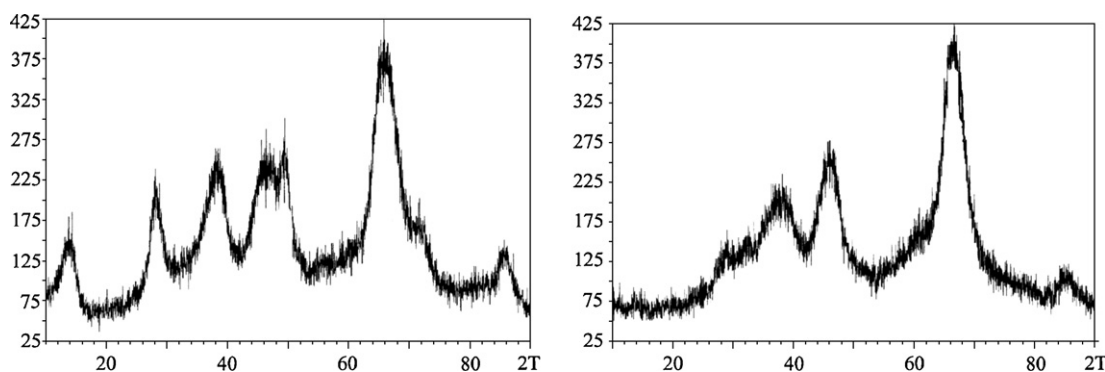


Fig. 2. XRD patterns of boehmite calcined at 250 °C for 24 h: (left, BCT₂₅₀NV) under atmosphere (right, BCT₂₅₀LV) under 0.01 bar.

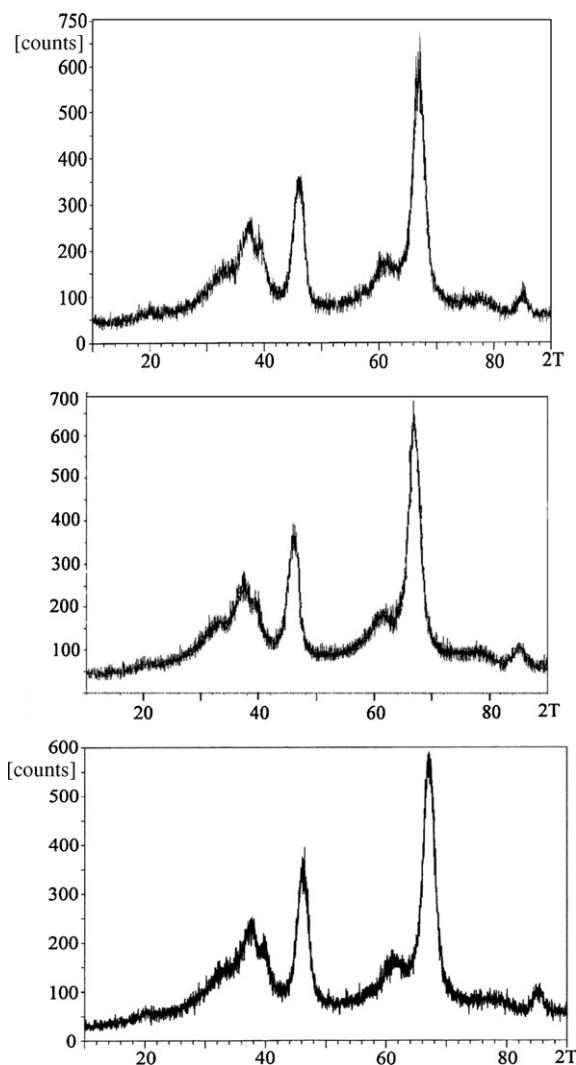


Fig. 4. XRD spectrums of boehmite calcined at 600 °C under different pressures: one atmosphere (top); low vacuum (middle); high vacuum (bottom).

be closer to γ -Al₂O₃ model than the boehmite (BCT₁₂₀NV) sample.

The XRD spectra of boehmite calcined at 350 °C (BCT₃₅₀NV and BCT₃₅₀LV) are not quite similar to the pattern observed for a defined γ -Al₂O₃ structure; however, the main peaks, that are characteristic of γ -Al₂O₃, did appear (Fig. 3). The only difference observed was that the two small peaks at $2\theta \approx 39^\circ$ and $2\theta \approx 62^\circ$ were not fairly apparent as they lied in the γ -Al₂O₃ spectrum. The XRD patterns of boehmite calcined at 600 °C (BCT₆₀₀NV) (Fig. 4) show the entire characteristic features of γ -Al₂O₃ as reported in the literature [4,55–58].

A qualitative measure of crystallinity and particle size was obtained based on peak heights and peak widths of $2\theta \approx 67^\circ$. A decrease in peak widths was observed with an increase in temperature. Similarly, a decrease in peak height was observed under reduced pressure at a constant calcination temperature, which is a good indication of low crystallinity (Fig. 4).

3.2. Infrared spectra

FT-IR technique was used to help obtain a thorough understanding of the structural features of the prepared catalysts. For instance, identification of adsorbed water, determination of the amount of OH groups present on the surface, and evaluation of

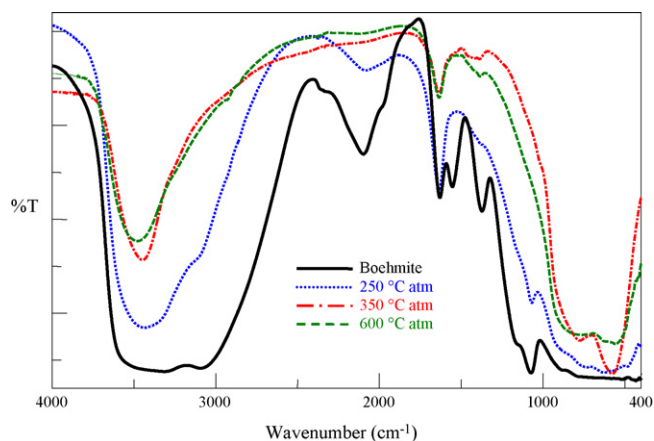


Fig. 5. FT-IR spectra of boehmite calcined at temperatures 120, 250, 350, and 600 °C under atmospheric pressure.

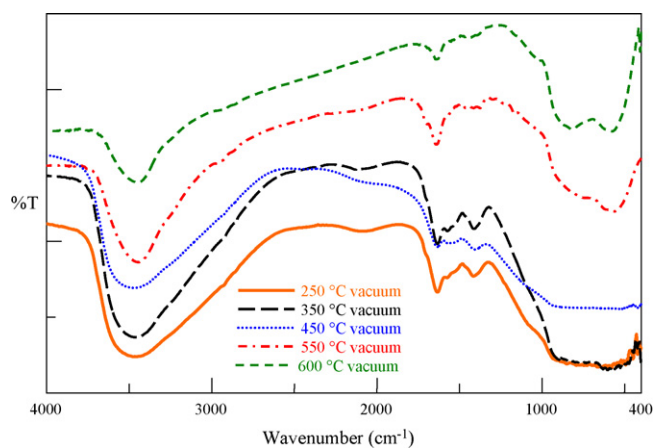


Fig. 6. FT-IR spectra of boehmite calcined at different temperatures under 0.01 bar.

Al–O–Al bonds developed resulted from catalyst dehydroxylation.

The FT-IR spectrum of boehmite (Fig. 5) clearly shows a broad OH stretching mode from 2500 to 3840 cm⁻¹, which stands for surface hydroxyls and adsorbed water. The peaks at 1072 cm⁻¹ and a shoulder at 1166 cm⁻¹ follow from the Al–O–Al asymmetric and symmetric bending modes. The observed decrease in the OH peak region is a good indication of the temperature effect on the dehydroxylation process. As we will conclude from thermal analysis experiments below, dehydroxylation and γ -Al₂O₃ formation are two events taking place as a result of boehmite thermal treatment. The decrease in the OH peak area and the peaks developing between 500 and 1000 cm⁻¹ an indication of ν -AlO₄ and ν -AlO₆ are convincing evidences supporting TGA and DTG (predicts significant water loss at 250–491 °C). Several publications have addressed the hydroxyl surface of alumina using IR spectroscopy [56,59,60]. The IR spectra of boehmite calcined at 600 °C under reduced pressure (0.01 and 1×10^{-6} bar) show large reduction of hydroxyl group (major loss of water at 250–350 °C) and appearance of a small peak at 1023 cm⁻¹ (Al–O–Al bending vibrations) (Figs. 6 and 7). This peak is absent in the spectrum for alumina prepared under atmospheric pressure. This is an indication of morphologic alteration. Formation of Al–O–Al bond might be a consequence of the condensation of two OH groups lying on a particle's pore surface (inner-structure change) or two hydroxyls located on the outer surface of two different alumina particles (larger γ -Al₂O₃ particles). Reactivity and selectivity data (Section 3.6) predicts the latter case to be the dominating factor under vacuum.

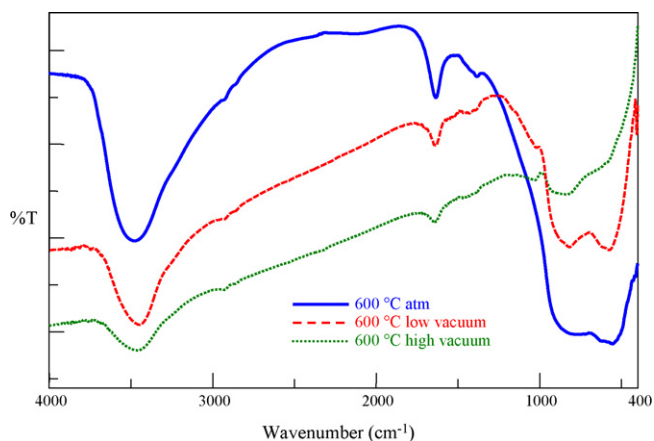


Fig. 7. FT-IR spectra of boehmites calcined at 600 °C under atmosphere (top), 0.01 bar (middle) and 1×10^{-6} bar (bottom).

3.3. SEM studies

In order to find proof for the possible morphologic changes, as already considered in the FT-IR study, SEM images of BCT₆₀₀HV and BCT₆₀₀NV were recorded at a magnification of 33,872 \times (Fig. 8), in which the effect of reduced pressure on particle size is apparent. While particle size change confirms our idea about external surface hydroxyl condensation, condensation of inner surface hydroxyls is still possible. One can notice that lower water vapor pressure under vacuum simply facilitates dehydroxylation, including also the external OH groups. Another explanation which was inferred from the SEM images is that when particles gain energy during calcinations, the air present between particles is an effective factor in reducing particle energy. When air is sucked out by the vacuum pump, there is no fluid available for particles to collide with. Consequently, the only way for particles to transfer their energy is to have collisions with each other. The more the collisions, the greater is the possibility for particle size growth. The role of collision is to bring two external OH groups closer and to increase the chances for water loss and creation of an Al–O–Al bond.

3.4. BET analysis

The Brunauer–Emmett–Teller (BET) specific surface area for the boehmite (BCT₁₂₀NV) was measured 352.0 m²/g. This value for catalysts BCT₂₅₀LV, BCT₃₅₀NV, BCT₃₅₀LV, BCT₆₀₀NV, BCT₆₀₀LV, and BCT₆₀₀HV was measured 242.7, 246.2, 273.2, 150.0, 164.5 and 179.4 m²/g, respectively. These results indicate that the surface area of boehmite drastically was reduced at 250 °C (calcinations temper-

ature). The surface area for γ -Al₂O₃ was increased under reduced pressure.

3.5. Thermal analysis

Thermal analysis was performed both to evaluate the thermal behavior of boehmite and to collect more information on the dehydration process during catalyst preparation. Alphonse and Courty pointed out that four steps taken into consideration in thermally stimulated transformation of nanocrystalline boehmite into alumina [57]. Bokhimi et al. recorded DTA curves of various boehmites and observed two endothermic and one exothermic peak. The two endothermic peaks corresponded to water desorption and boehmite transition to alumina, respectively. The exothermic peak that appeared at above 1100 °C was assigned to α -Al₂O₃ formation [61].

In this research, the TG and DTG curves were recorded in the temperature range between 22 and 1200 °C. A significant weight loss was observed at temperatures between 200 and 500 °C (IR predicts major loss of water at 250–350 °C). This temperature range encompasses important thermal processes such as transition alumina creation which starts below 300 °C (Figs. 9 and 10). Examination of the DTG diagram justifies the conclusion that the imperative changes during boehmite heat treatment include physisorbed water desorption, chemisorbed water desorption, and formation of γ -Al₂O₃. Depending on the starting aluminum oxyhydroxide, treatment at higher temperatures could result in more dehydroxylation, appearance of other transition aluminas, and, finally at above 1100 °C, formation of a α -Al₂O₃. These thermal findings complement the FT-IR data presented above which also indicated the phase transformation at higher temperature or under reduced pressure.

Interpretation of the DTG pattern indicates that boehmite transformation to γ -Al₂O₃ begins at around 240 °C and comes to an end at 491 °C. It is apparent that the highest rate of dehydroxylation occurs at 402 °C (Fig. 10).

3.6. Effect of calcination temperature and vacuum on catalyst activity and selectivity

Reaction of 1,2-diphenyl-2-propanol (DPP) in 96% 2-octanol was examined over calcined catalysts (BCT₂₅₀NV, BCT₂₅₀LV, BCT₃₅₀NV, BCT₃₅₀LV, BCT₆₀₀NV, BCT₆₀₀LV, and BCT₆₀₀HV) at a flow rate of 18 cm³/h at 280 °C on a Pyrex vertical flow reactor. 2-Octanol was used as the solvent and, more importantly, as an isomerization preventer. Results are summarized in Tables 1–3. Furthermore, reaction of 2-octanol helped us to gain important information on the dehydration of secondary alcohols. Elimination reactions of alcohols were carried out under identical conditions including tem-

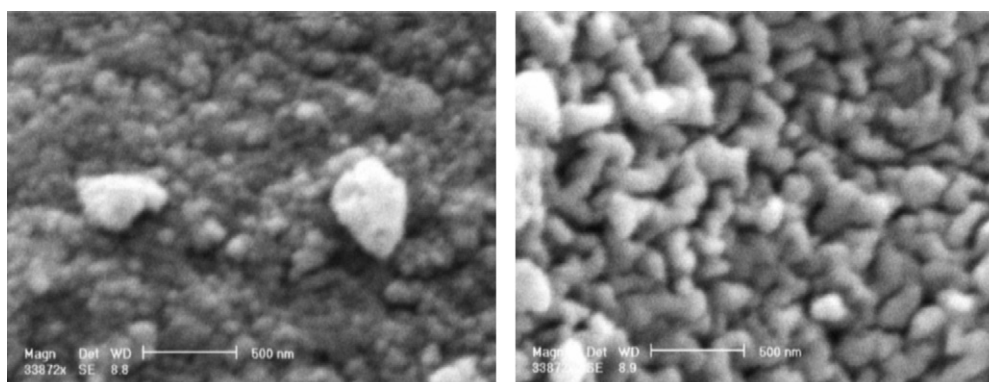


Fig. 8. SEM images of BCT₆₀₀NV (left) and BCT₆₀₀HV (right).

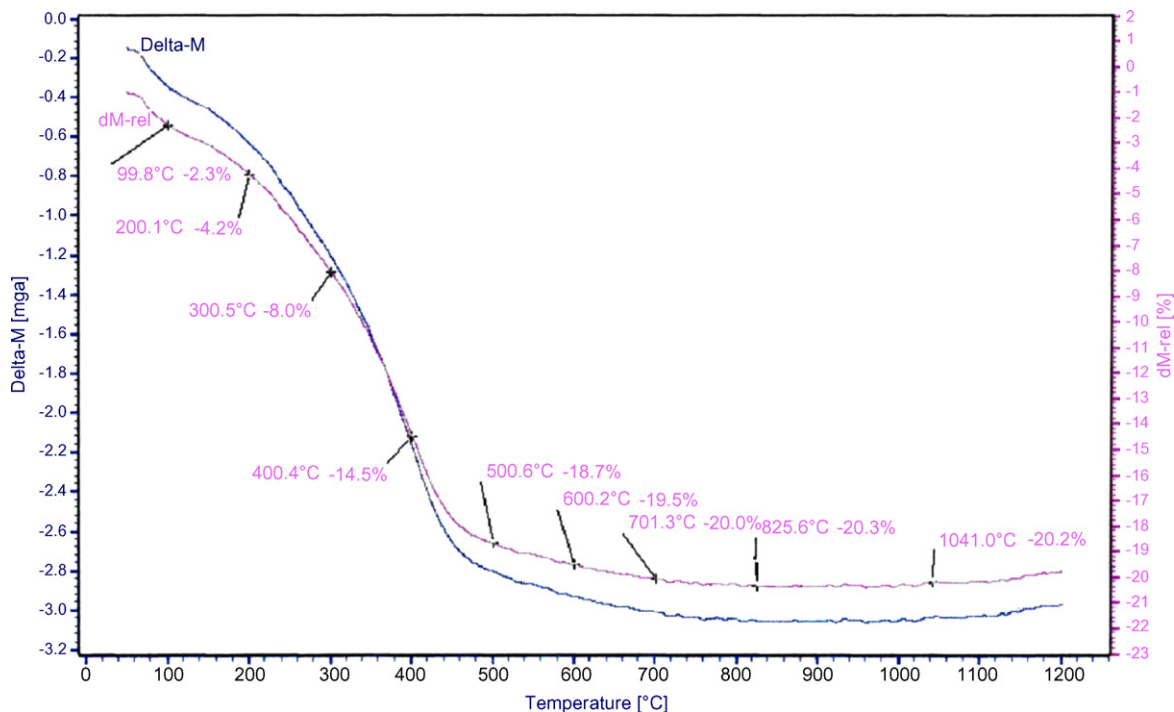


Fig. 9. TG curve recorded for boehmite (mass = 15 mg, heating rate = 10 °C/min).

perature (280 °C with the exception of the catalysts which were calcined at 250 °C for which the reaction temperature was kept at 250 °C), mesh size, flow rate, amount of catalyst, concentration, and reactor type.

The questions raised here include whether the reaction of aluminum oxide (prepared under vacuum and/or different calcination

temperatures) with secondary alcohol (2-octanol) and tertiary alcohols (DPP) affects the dehydration reaction. If so, what would then be the mechanism of elimination for these reactions? What would the effect of vacuum be on the structure and morphology of the catalysts? To answer these questions, we studied the effects of changes in vacuum pressure and calcination tempera-

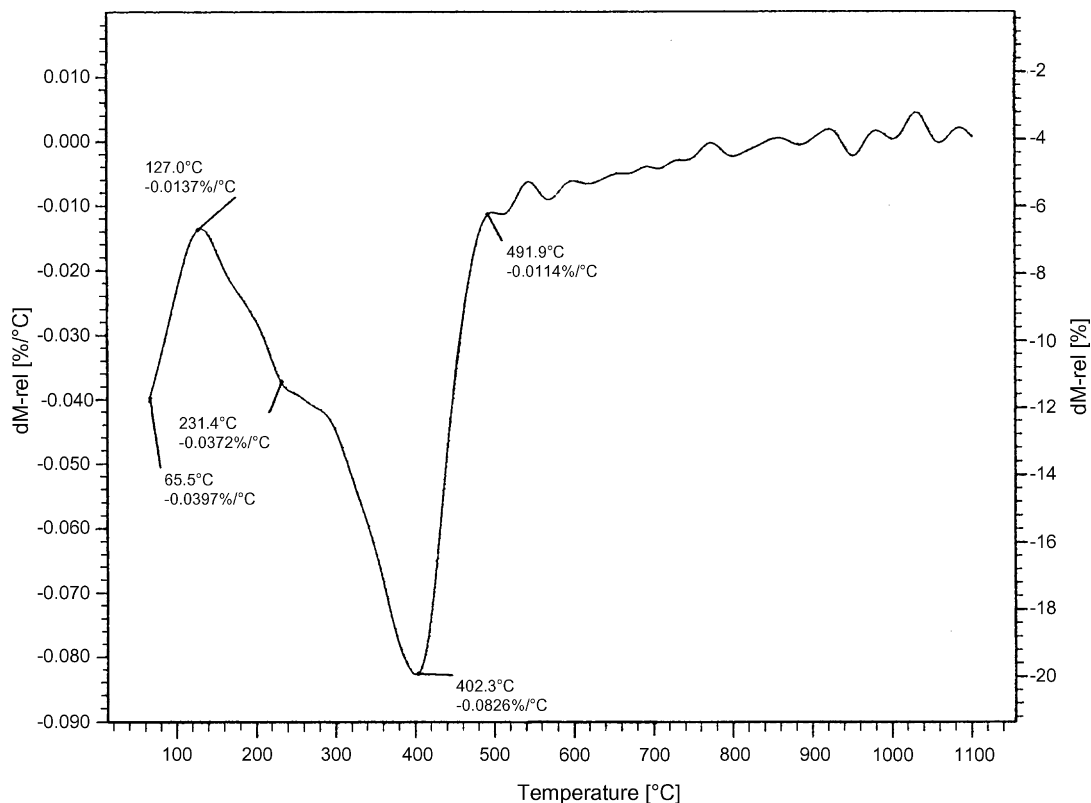


Fig. 10. DTG curve recorded for boehmite (mass = 15 mg, heating rate = 10 °C/min).

Table 1
Effect of calcinations temperature on alcohol conversions under one atmosphere or vacuum at 280 °C.

Catalyst	2-Octanol% ^a	DPP%	DPP/2-octanol
BCT ₂₅₀ NV ^b	27	89	3.3
BCT ₂₅₀ LV ^b	41	100	2.4
BCT ₃₅₀ NV	50	95	1.9
BCT ₃₅₀ LV	44	96	2.2
BCT ₆₀₀ NV	47	97	2.1
BCT ₆₀₀ LV	64	99	1.5
BCT ₆₀₀ HV	46	97	2.1

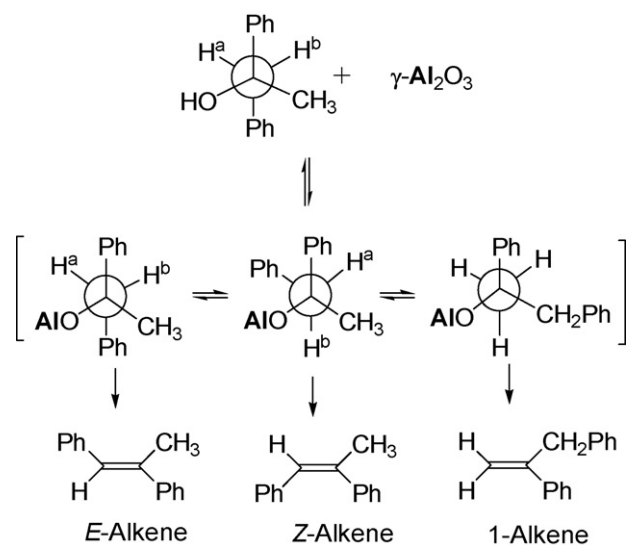
^a Percent calculated by GC.

^b Reactions were carried out at 250 °C.

Table 2
Effect of calcinations temperature on product distribution of dehydration of DPP under one atmosphere or vacuum at 280 °C.

Catalyst	1-Alkene	E-2-Alkene	Z-2-Alkene	1-Alkene/ 2-alkenes	E/Z
BCT ₂₅₀ NV ^a	60.80	22.46	16.73	1.55	1.34
BCT ₂₅₀ LV ^a	57.37	17.10	25.53	1.34	0.67
BCT ₃₅₀ NV	46.14	33.73	20.13	0.86	1.68
BCT ₃₅₀ LV	50.29	31.40	18.30	1.01	1.72
BCT ₆₀₀ NV	46.18	36.14	17.68	0.86	2.04
BCT ₆₀₀ LV	49.12	34.28	16.78	0.96	2.04
BCT ₆₀₀ HV	48.42	32.91	18.67	0.94	1.76

^a Reactions were carried out at 250 °C.



Scheme 1. Schematic representation of DPP dehydration reaction.

ture on reactivity (conversion of alcohols), stereoselectivity (e.g., the ratio of syn/anti-elimination), regioselectivity (e.g., the ratio of Saytzeff/Hofmann elimination), and the structure of the catalysts.

Conversions of 27, 50, 47% (for 2-octanol) and 89, 95, 97% (for DPP) were obtained under one atmosphere at 250, 350, and 600 °C,

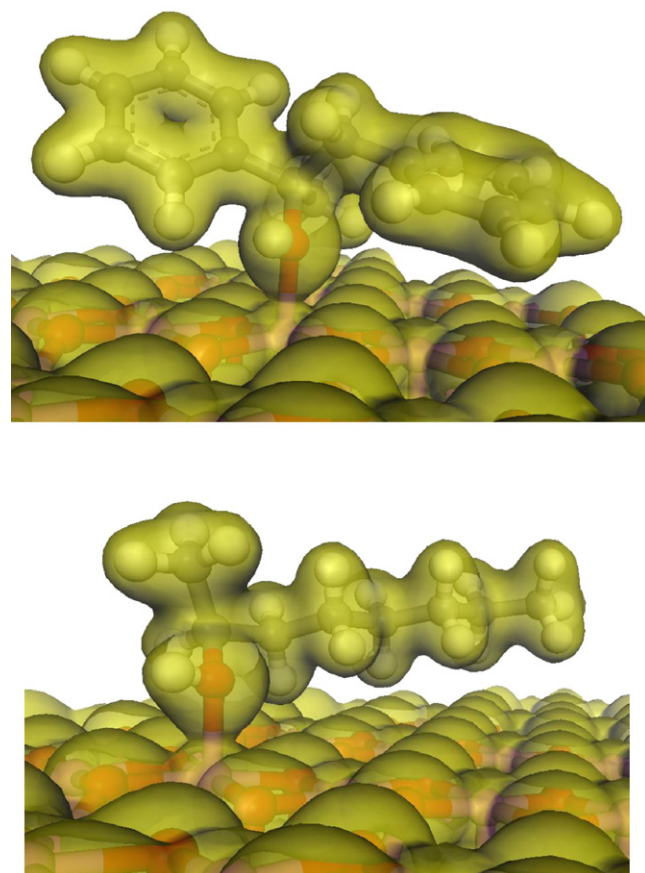


Fig. 11. Total electron density of alumina (100) surface after adsorption of the most stable conformer of R-DPP (top) and S-2-octanol (bottom).

respectively (Table 1). Generally, tertiary alcohols reacted faster (formation of a stable 3° cation) than secondary alcohols under E1 elimination. We concluded that the elimination reactions of tertiary and secondary alcohols over $\gamma\text{-Al}_2\text{O}_3$ proceeds through E2 mechanism [25,26,62]. Then, what other factor(s) may be involved in controlling the very high conversion rate of DPP over 2-octanol? One may assume the stronger adsorption of DPP plays a major part. The interaction of the two phenyl groups with the surface favors the conversion of DPP. The repulsion of long chain octyl moiety lowers the conversion.

Reactivity and selectivity (E/Z, trans/cis and 1-alkene/2-alkenes) were slightly improved under reduced pressure for both alcohol dehydration with the exception of catalysts calcined at 250 °C (27% conversion of 2-octanol under no vacuum; 41% under vacuum) and for catalyst BCT₆₀₀LV higher conversion (64%) of 2-octanol was observed under low vacuum (47% under no vacuum). The cis/trans ratio of 4.2, 3.0, 3.1 and 2 was measured for 2-octanol over BCT₂₅₀LV, BCT₃₅₀LV, BCT₆₀₀HV and BCT₆₀₀NV, respectively. Isomerization (formation of 3-octenes) was decreased for the catalysts

Table 3
Effect of calcinations temperature on product distribution of dehydration of 2-octanol under one atmosphere or vacuum at 280 °C.

Catalysts	1-Octene	t-2-Octene	c-2-Octene	3-Octene	1-Ene/2-ene	Cis/trans	Diocetyl ether A	Diocylether B
BCT ₂₅₀ NV ^a	37	13	46	0.23	0.6	3.7	2.2	2.15
BCT ₂₅₀ LV ^a	38	11	45	0.11	0.7	4.2	3.0	3.18
BCT ₃₅₀ NV	30	19	48	2.7	0.4	2.5	0.2	0.20
BCT ₃₅₀ LV	31	17	50	2.0	0.5	3.0	0.4	0.32
BCT ₆₀₀ NV	26	23	46	4.0	0.4	2.0	0.2	0.17
BCT ₆₀₀ LV	30	19	48	1.2	0.5	2.5	0.6	0.55
BCT ₆₀₀ HV	31	16	50	2.3	0.5	3.1	0.3	0.31

^a Reactions temperature at 250 °C.

Table 4
Relative energy, ΔE_{rel} (kcal/mol), of alcohol conformers over the (100) and (110) surfaces of alumina before and after adsorption, adsorption energy, and the $\text{Al}_{\text{alumina}}-\text{O}_{\text{alcohol}}$ (Al–OHR) bond distance (Å); values in parentheses are related to (110) surface.

Conformers	ΔE_{rel} (kcal/mol) before adsorption	ΔE_{rel} (kcal/mol) after adsorption	Adsorption energy (kcal/mol)	$\text{Al}_{\text{alumina}}-\text{O}_{\text{alcohol}}$ distance (Å)
(S)-2-Octanol				
1a	0.871	0.000 (0.757)	–38.227 (–62.890)	2.051 (1.985)
1b	0.871	1.032 (2.339)	–37.195 (–61.308)	2.043 (1.901)
1c	0.342	12.693 (24.124)	–25.005 (–38.995)	2.052 (1.914)
1d	0.000	5.247 (0.000)	–32.109 (–62.776)	2.082 (1.928)
(R)-2-Octanol				
2a	0.000	0.907 (6.332)	–32.021 (–60.939)	2.072 (1.916)
2b	0.342	3.292 (25.721)	–29.977 (–41.891)	2.091 (1.931)
2c	0.871	0.000 (0.000)	–33.800 (–68.143)	2.072 (2.051)
(S)-DPP				
3a	0.000	8.447 (4.252)	–37.947 (–61.448)	2.178 (1.981)
3b	0.014	1.875 (0.000)	–43.365 (–64.547)	2.128 (1.904)
3c	1.419	0.000 (23.818)	–46.945 (–42.433)	2.130 (2.198)
(R)-DPP				
4a	0.000	0.000 (1.924)	–49.382 (–72.447)	2.082 (1.964)
4b	0.014	1.165 (0.000)	–44.320 (–74.385)	2.064 (1.980)
4c	1.419	7.467 (19.703)	–39.354 (–56.087)	2.293 (2.024)

prepared at 250 °C under vacuum and was increased for catalyst BCT₆₀₀NV. Ether formation was increased for catalysts calcined at lower temperatures under vacuum (Scheme 1 and Table 2).

There are several reactions that may proceed under vacuum at elevated temperature. Obviously, more hydroxyls group are lost (loss of water) under vacuum which could enhance an increase in the number of cross-links. These links could form new bonds within the alumina particle (intraparticle cross-links, formation

of smaller pores and crevices) and/or between the adjacent particles (interparticles cross-links) which make larger particle size (see SEM under high vacuum). Initially we assumed that the former should make the catalyst more selective. Catalyst with smaller pores or crevices should be more selective toward reacting with larger molecules. However, much smaller change in activity and selectivity was observed than it was anticipated. Apparently, the small number of pores and crevices formed under vacuum can-

Table 5
The distance between eliminable hydrogens and basic sites of the (100) and (110) alumina surfaces.

Conformers	Eliminable hydrogens	Distance (Å)		Product
		(100)	(110)	
(S)-2-Octanol				
1a	H _α	2.616	4.220	2-Octanone
	H _β	2.656, 3.014, 3.067	3.044	cis-2-Octene
	H _{β'}	4.107, 4.306	–	cis-2-Octene
1b	H _α	3.102	2.740, 2.953	2-Octanone
	H _{β''}	2.545, 3.859	3.556, 3.816	1-Octene
1c	H _α	3.845	3.814	2-Octanone
	H _β	2.633, 2.993	3.443	cis-2-Octene
	H _{β'}	2.586, 2.931, 3.349	2.988	trans-2-Octene
1d	H _{β''}	4.021, 4.338	4.201, 4.298	1-Octene
	H _α	3.809	–	2-Octanone
	H _{β'}	3.522, 3.873	2.693, 3.483	trans-2-Octene
	H _{β''}	–	3.239, 3.709	1-Octene
(R)-2-Octanol				
2a	H _β	3.422, 3.455, 4.080	2.689, 3.474	trans-2-Octene
	H _{β''}	3.765, 3.858	3.896, 4.005	1-Octene
2b	H _β	2.788, 3.151, 3.498	2.993, 3.415	trans-2-Octene
	H _{β'}	2.532, 3.044	3.606	cis-2-Octene
2c	H _{β''}	2.799, 3.169, 3.752	–	1-Octene
	H _{β'}	4.419, 4.633	3.872, 4.412	cis-2-Octene
	H _{β''}	2.623, 3.239, 3.400	3.311, 3.493, 3.851	1-Octene
(S)-DPP				
3a	H _β	3.617, 3.687	3.641, 4.247	E-2-Alkene
	H _{β''}	3.810	3.763, 4.192	1-Alkene
3b	H _β	2.589, 3.673, 3.958	2.773, 3.962	E-2-Alkene
	H _{β'}	4.117, 4.456	2.523, 2.837	Z-2-Alkene
3c	H _{β''}	2.945, 3.064, 3.381, 3.094	4.286, 4.348	1-Alkene
	H _{β'}	2.620, 3.937, 3.837	4.487	Z-2-Alkene
	H _{β''}	2.396, 3.553, 3.351	4.058, 4.253	1-Alkene
(R)-DPP				
4a	H _{β''}	2.653, 2.769, 3.327, 3.415	2.609, 2.735, 3.480, 3.536	1-Alkene
4b	H _β	4.315, 4.442	4.571	Z-2-Alkene
	H _{β'}	4.423	4.529	E-2-Alkene
4c	H _{β''}	3.261, 3.667, 3.113	3.150, 3.082, 3.536	1-Alkene
	H _{β'}	3.433, 4.003, 4.072	3.679, 3.846	1-Alkene

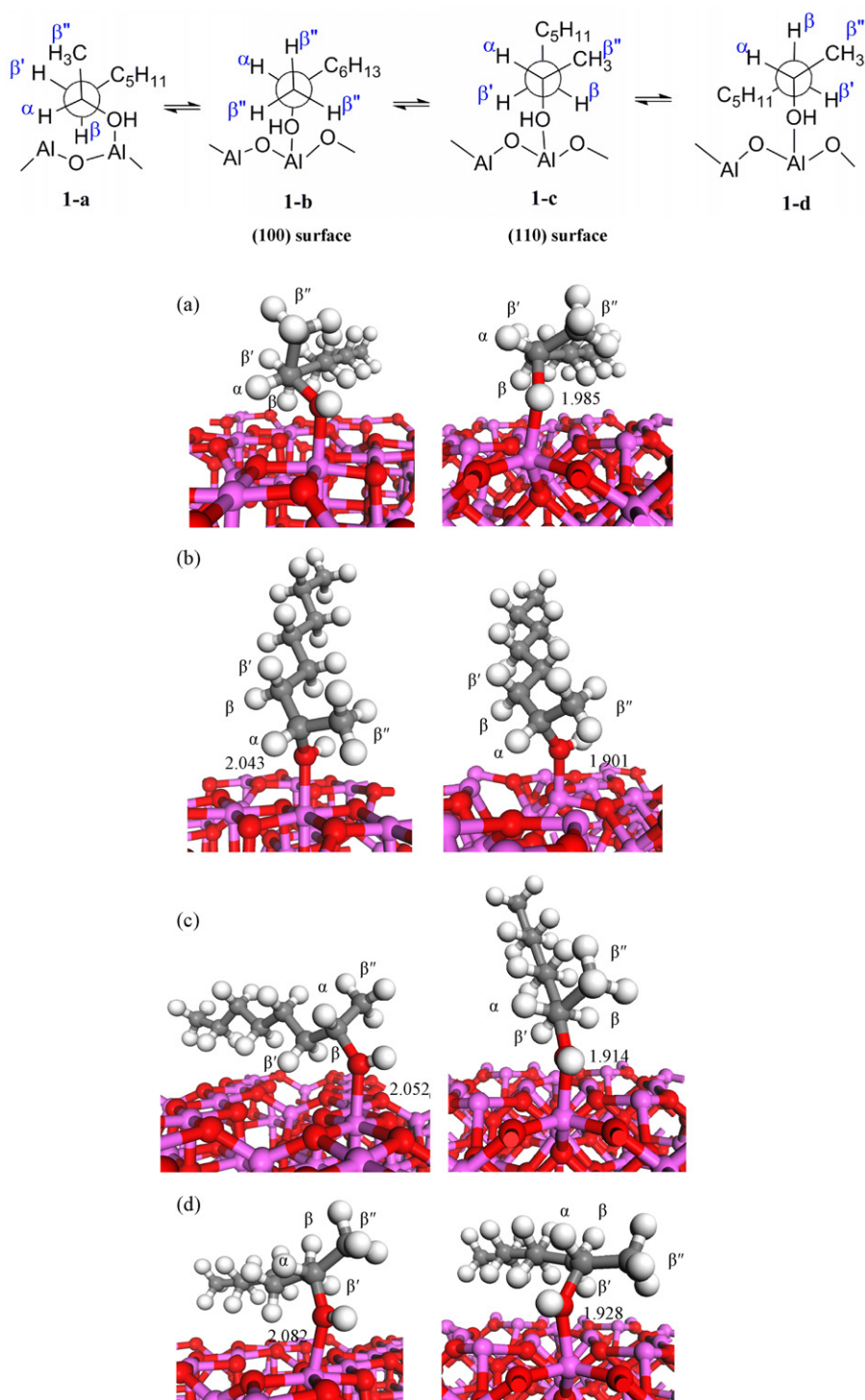


Fig. 12. Portion of S-2-octanol conformers over (100) and (110) alumina surfaces.

not compete with medium and large size pores and crevices which control the overall reactivity and selectivity of the bulk alumina.

3.7. Quantum chemical calculation

The adsorption of alcohols over γ - Al_2O_3 was investigated by several research groups [34,54,63]. The adsorption of methanol was studied by De Vito et al. [63]. They concluded that methanol adsorbs on a tetrahedral aluminum ion forming a covalent bond. Cai and Sohlberg [34] computed the adsorption of methanol, ethanol, propanol, and isopropanol over the γ - Al_2O_3 (110) surface. They

showed that all four alcohols chemisorb over the alumina surface when they come sufficiently close to the surface with proper orientation. Feng et al. [54] have presented a detailed theoretical study on isopropanol adsorption on both clean and hydrated γ - Al_2O_3 (100) and (110) surfaces. All possible adsorption configurations were considered in their calculation.

In this study computation of the optimized geometry of the defect spinel alumina predicted an unsymmetrical (100) and (110) surfaces. This promoted an investigation of the effect of the stereochemistry (*R* or *S* configuration) of the adsorbed chiral alcohol over the unsymmetrical surfaces (Figs. 11–15). This raises the ques-

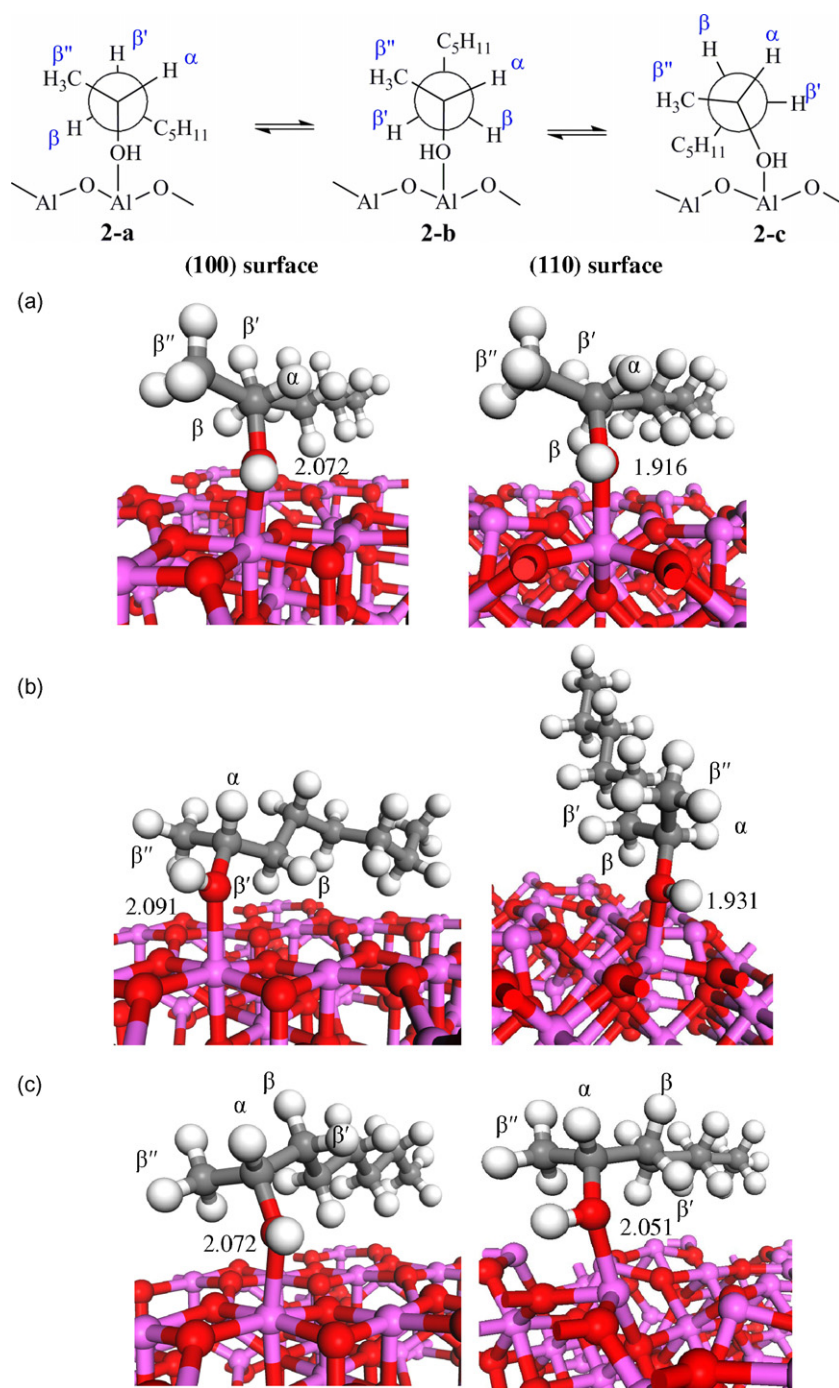


Fig. 13. Portion of *R*-2-octanol conformers over (100) and (110) alumina surfaces.

tion, whether; the surface with the adsorbed chiral alcohol could produce diastereoselective property.

Two additional questions were raised earlier regarding the factors controlling the conversion (reactivity) and product distribution (selectivity) of 2-octanol and DPP over γ - Al_2O_3 . These questions can now be satisfactorily answered along the following lines. The low conversion of the former alcohol is related to the repulsion of the long chain octyl group from the surface. The high conversion of the latter alcohol is presumed to be a result of strong adsorption of DPP over the surface. The pi-electron clouds of phenyl groups interact with the surface stabilizing the acidic sites ($\text{Al} \cdots \pi$ interactions [64]). The $\text{Al} \cdots \pi$ interaction is defined as the attraction between a

Lewis acid site and the face of a simple π system with an electrostatic origin. These interactions stabilize the alumina surface and they are more important than the weak $\text{C-H} \cdots \text{Al}$ or $\text{C-H} \cdots \text{O}$ interactions of octyl moiety. Fig. 11 shows the total electron density of γ - Al_2O_3 (100) surface after adsorption of the most stable conformer of *R*-DPP and *S*-2-octanol. In the former alcohol two $\text{Al} \cdots \pi$, two $\text{O} \cdots \pi$, seven $\text{C-H} \cdots \text{O}$ and a $\text{C-H} \cdots \text{Al}$ distances are almost 3.8, 4.6, 3.4, 4.1, 2.6, 2.8, 3.0, 4.3, 3.4, 3.5, 2.7 and 3.2 Å, respectively. For the latter alcohol two $\text{C-H} \cdots \text{Al}$ and six $\text{C-H} \cdots \text{O}$ distances are 3.3, 4.4, 2.6, 3.2, 2.9, 3.3, 2.9 and 3.6 Å, respectively.

A third question raised involved the reason for this state of affairs, which might be answered now along the following lines: the

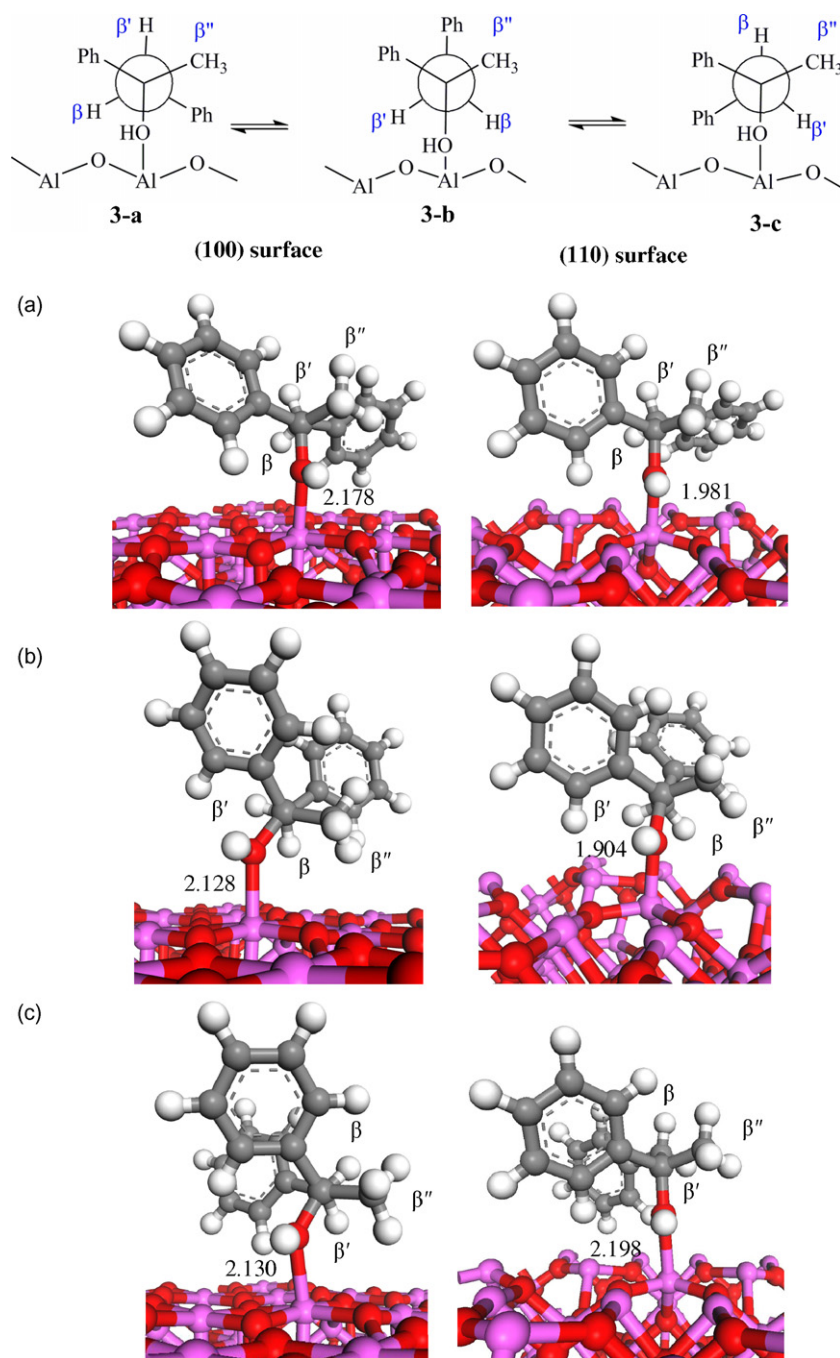


Fig. 14. Adsorption of S-DPP conformers over (100) and (110) alumina surfaces.

major product of 2-octanol is *cis*-2-alkene but for DPP it is 1-alkene. And the last question awaiting an answer is 'what is the effect of the configuration of a chiral alcohol on the adsorbed species and on product distribution of the elimination reaction?'

In this section, these questions are confronted using density functional theory. The calculated adsorption energy, bond length, relative energy of the title alcohol conformers before and after adsorption (ΔE_{ads}) and the probable products of elimination are shown in Tables 4 and 5 and in Figs. 12–15.

The method predicted a lower adsorption energy for the adsorbed 2-octanol (in the range of -25 to -38 kcal/mol, Figs. 12 and 13) than for the adsorbed DPP (in the range of -38 to -49 kcal/mol) (Figs. 14 and 15) over the (100) surface. In other words, the more negative adsorption energy value indicates stronger adsorption of alcohol over the surface. The phenyl groups

of DPP with a high electron density adsorb more strongly over the surface than the long chain of 2-octanol. The adsorption energy of 2-octanol conformers over the (110) surface are in the range of -39 to -68 kcal/mol. These values are higher than those obtain over the (100) surface. This difference is related to the nature of alumina surface. The upper layer of (100) surface is formed by penta-coordinated aluminum atoms; while (110) surface has both tri- and tetra-coordinate geometry. The tri-coordinated aluminum atoms of the (110) surface are stronger Lewis acids than penta-coordinated aluminum atoms [39]. These results complement the prediction of Feng et al. [54] about the adsorption of isopropanol over the (100) and (110) surfaces. They concluded that isopropanol was adsorbed better over the (110) surface ($\Delta E_{\text{ads}} = -45.588$ kcal/mol versus -20.100 kcal/mol). In the case of DPP conformers, the adsorption energy over the (110) sur-

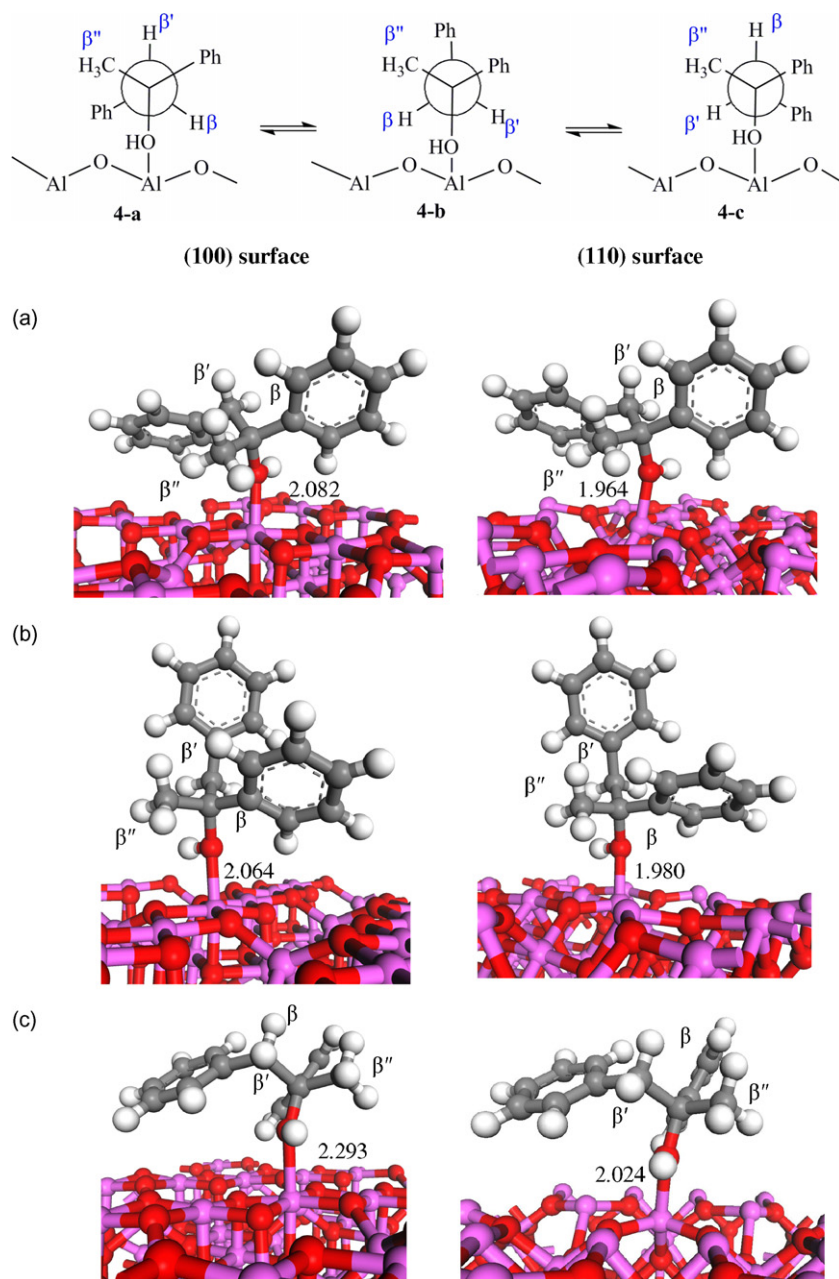


Fig. 15. Adsorption of *R*-DPP conformers over (100) and (110) alumina surfaces.

face (tri-coordinated aluminum atoms) is in the range of -42 to -74 kcal/mol. These results indicated that the most stable conformers of DPP have higher adsorption energy over the (110) surface than the (100) with the exception of conformer **3b** (Fig. 14b).

Bond distances (Al–OHCR) of the adsorbed (*S*)-2-octanol conformers over the (100) surface were calculated 2.051, 2.043, 2.052, and 2.082 (Fig. 12a–d), respectively, and 2.072, 2.091, and 2.072 (Fig. 13a–c) for (*R*)-2-octanol, respectively. The corresponding values over (110) surface are 1.985, 1.901, 1.914 and 1.928 for (*S*)-2-octanol, and 1.916, 1.931 and 2.051 for (*R*)-2-octanol conformers, respectively.

The relative energy of 2-octanol conformers (listed in Table 4) predicts that the most stable conformation of the adsorbed alcohol over (100) or (110) surface is different from that of the most stable conformation of a free alcohol. For instance, the most stable conformer of free and adsorbed alcohol over (100) and (110) surface is **1d** (CH_3 and C_5H_{11} groups are anti), **1a** (CH_3 and C_5H_{11} groups

are gauche) and **1d** for (*S*)-stereo isomer and is **2a** (CH_3 and C_5H_{11} groups are anti), **2c** (CH_3 and C_5H_{11} groups are gauche) and **2c** for (*R*)-2-octanol (Figs. 12 and 13).

Bond distances (Al–OHCR) between the oxygen atom of the adsorbed alcohol and alumina (100) surface for the three (*S*)-DPP conformers **3a**, **3b**, and **3c** were calculated to be 2.178, 2.128, and 2.130 Å with adsorption energy values of -37.947 , -43.365 , and -46.945 kcal/mol, respectively (Fig. 14a–c). These bond distances for (110) surface are 1.981, 1.904 and 2.198 Å with adsorption energy values of -61.448 , -64.547 , and -42.433 kcal/mol, respectively. The most stable conformer of free and adsorbed alcohol over (100) and (110) surface is **3a** (two phenyl groups are anti), **3c** (two phenyl groups are gauche) and **3b** (two phenyl groups are gauche) for (*S*)-stereo isomer (Figs. 14 and 15). The longer bond distance and the lower adsorption energy were obtained for the conformer **3a** (which the two phenyl groups are anti) over (100) surface, while the reverse of this observation was calculated for (*R*)-

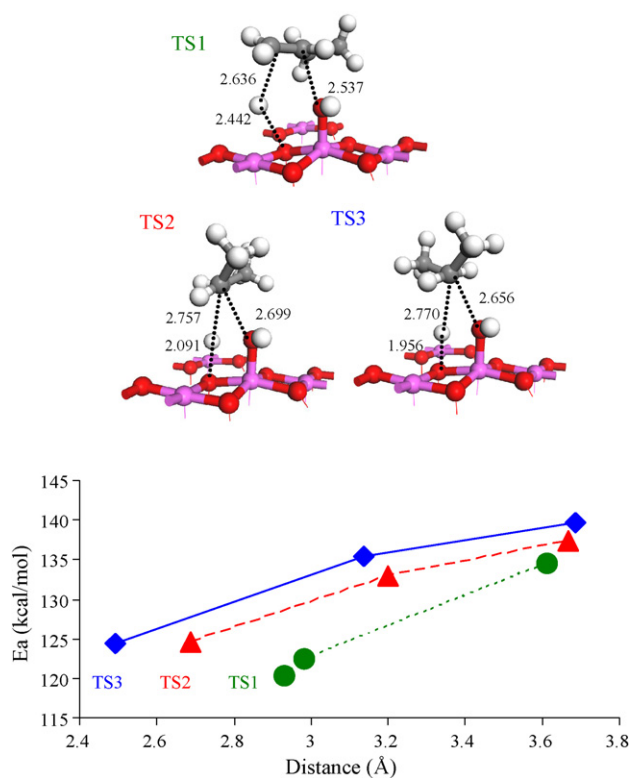


Fig. 16. Correlation between activation energy [for three path of products formation: 1-butene (●), cis-2-butene (▲) and trans-2-butene (◆)] and distance of $O_{\text{alumina}}-H_{\beta}$ 2-butanol.

DPP that predicted the **4a** conformer (which two phenyl groups are anti) has maximum of adsorption energy. Bond distances between the oxygen atom of the adsorbed alcohol and alumina (RCHO–Al) for the three (*R*)-DPP conformers **4a**, **4b**, and **4c** over (1 0 0) surface were calculated to be 2.082, 2.063, and 2.292 Å with adsorption energy (ΔE_{ads}) values of –49.382, –44.320, and –39.354 kcal/mol, respectively (Fig. 15a–c). These bond distances for (1 1 0) surface are 1.964, 1.980 and 2.024 Å with adsorption energy values of –72.447, –74.385 and –56.087 kcal/mol, respectively.

Investigating the transition state (TS) for large molecules (DPP or 2-octanol) requires super computer and state of art software and time. Therefore, 2-butanol was used in this work as a model molecule for describing the transition states and correlation between the activation energy and the distances of basic sites of alumina and eliminable hydrogens (β , β' and β'') of alcohol. These results help shed some light on the elimination reaction pathway (starting material (2-butanol/ γ - Al_2O_3) \rightarrow transition state $[\text{TS}]^\ddagger \rightarrow$ products) over each basic site of the alumina surface. It should be mentioned that calculation of transition states for 2-butanol conformers is simple, because one need very small surface area of alumina (containing 30 atoms, $\text{Al}_{16}\text{O}_{24}$) to gain complete interaction of alcohol with the surface. A very large surfaces ($\text{Al}_{64}\text{O}_{96}$ for (1 0 0) and $\text{Al}_{48}\text{O}_{64}$ for (1 1 0)) were required for calculating the activation energy for DPP or 2-octanol dehydration.

The correlation between activation energy (E_a) and the distance between basic sites and eliminable hydrogens are shown in Fig. 16. E2 elimination of $H_{\beta''}$ of (*R*)-2-butanol via a basic site of alumina produces 1-butene (TS1). E2 elimination of β and β' hydrogens of (*S*)-2-butanol leads to the formation of cis (TS2) and trans (TS3) products, respectively. The activation energy of 1-butene formation is smaller than that of the corresponding value for 2-butenes.

A general increase was observed for the activation energy for elimination of a β -hydrogens with increase in the distance between

β -hydrogen and basic site. Therefore, it was concluded that the adsorption of alcohol conformers over the surface and the distance between the basic sites and the eliminable hydrogens is a key step to understand the mechanism of alcohol dehydration. A comprehensive investigation is now under way.

The eliminable hydrogens are assigned α , β , β' , β'' and γ . The distances between each of the eliminable hydrogens from the basic site of the surface (Å) are listed in Table 5. For (*S*)-2-octanol, elimination of H_{β} and $H_{\beta'}$ from conformer **1a** and H_{β} from conformer **1c** (Fig. 12a and c) produced cis-2-octene (experimentally was produced as the major product). Elimination of $H_{\beta'}$ from conformer **1c** of *S*-enantiomer produced trans-2-octene. For (*R*)-2-octanol, elimination of two H_{β} from the conformers **2a** and **2b** (Fig. 13a and b) favored the formation of trans-2-octene. Elimination of $H_{\beta''}$ from the conformers **1b** and **1d** of *S*-enantiomer (Fig. 14b and d) and the conformers **2a**, **2b** and **2c** of *R*-enantiomer (Fig. 13a–c) produced 1-octene (Table 5). 2-Octanone is produced in very small amounts via elimination of H_{α} . γ -Elimination is less likely but possible in very small amounts via the four conformers **1a**, **1d** and **2a**, **2c** shown in Figs. 12a, d and a, c, respectively.

All six conformers of (*R*)- and (*S*)-DPP depicted in Figs. 14 and 15 produced 1-alkene (experimentally was reported as the major product). The conformer **3c** of (*S*)-DPP produced *Z*-alkene (experimentally was produced as the minor product). Figs. 14b and 15b both predict the formation of *E*- and *Z*-alkenes from the conformers **3b** and **4b** of DPP. However, elimination of H_{β} is favored to give *E*-isomer. The distance between H_{β} and the basic site of alumina is about 1 Å shorter than that between $H_{\beta'}$ (which gives *Z*-alkene) and the basic site.

The minimum distances between eliminable hydrogens (Table 5) and the oxygen of alumina (1 0 0) surface were found to be 2.396 Å (conformer **3c**) and 2.653 Å (conformer **4a**) leading to the 1-alkene from the most stable conformers. This distance over the (1 1 0) surface is 2.609 Å (conformer **4a**). The distance for the formation of *Z*-alkene and *E*-alkene over (1 0 0) surface are 2.620 (conformer **3c**), 2.589 (conformer **3b**) Å, respectively and over (1 1 0) surface are 2.523 (conformer **3b**), 2.773 (conformer **3b**) Å, respectively.

All of the quantum chemical calculations predict that (1 0 0) and (1 1 0) surfaces of defect spinel γ - Al_2O_3 with the adsorbed chiral alcohol have diastereoselective property. In other word, alcohols with (*R*)- or (*S*)- configuration behave differently over the surface. The experimental proof of this phenomenon is a challenge and remains to be investigated hopefully by us or other research group.

4. Conclusions

In summary, our results suggest that altering the boehmite's calcination conditions affects certain properties of alumina. XRD spectra show lower crystallinity for the catalysts prepared under reduced calcination pressure. The observed differences between the $\text{BCT}_{600}\text{NV}$ and $\text{BCT}_{600}\text{HV}$ XRD peak widths at $2\theta \approx 67^\circ$ were related to particle size change. This was verified by SEM. The BET surface area of the catalysts was increased when calcined under vacuum. A decrease in number of surface hydroxyls was obvious (by IR) as pressure declined at constant calcination temperature (600 °C).

Reactivity, stereoselectivity (*E/Z* or trans/cis) and regioselectivity (1-alkene/2-alkenes) were slightly increased under reduced pressure or at higher temperature for both alcohol dehydration with the exception of catalysts calcined at 250 °C and for catalyst $\text{BCT}_{600}\text{LV}$. The cis/trans ratio of 4.2, 3.0, 3.1 and 2 was measured for 2-octanol over $\text{BCT}_{250}\text{LV}$, $\text{BCT}_{350}\text{LV}$, $\text{BCT}_{600}\text{HV}$ and $\text{BCT}_{600}\text{NV}$, respectively. Isomerization was decreased for the catalysts prepared at 250 °C under vacuum (0.11%) and was increased for

catalyst BCT₆₀₀NV (4.0%). Ether formation was increased for catalysts calcined at lower temperatures under vacuum (6.18 for BCT₂₅₀LV and 0.61 for BCT₆₀₀HV).

Theoretical values complement the observed reactivity and selectivity. This method predicts that (100) and (110) surfaces with the adsorbed chiral alcohol show diastereoselective property.

The adsorption of alcohol conformers over the surface and the distance between the basic sites–eliminable hydrogens is a key step to understand the mechanism of alcohol dehydration.

Acknowledgements

We would like to thank Isfahan University of Technology (IUT) Research Council for their financial support (Grant # 86/500/9143). The authors are grateful to Dr. Abbas Teimuri and Professor Mohammad Ali Golozar for valuable discussions.

References

- [1] Y. Kim, C. Kim, P. Kim, J. Yi, J. Non-Cryst. Solids 351 (2005) 550–556.
- [2] J. Sanchez-Valante, X. Bokhimi, F. Hernandez, Langmuir 19 (2003) 3583–3588.
- [3] M.M. Amini, M. Mirzaee, J. Sol–Gel Sci. Technol. 36 (2005) 19–23.
- [4] Y.K. Park, E.H. Tadd, M. Zubris, R. Tannenbaum, Mater. Res. Bull. 40 (2005) 1506–1512.
- [5] L. Le Bihan, F. Dumeignil, E. Payen, J. Grimblot, J. Sol–Gel Sci. Technol. 24 (2002) 113–120.
- [6] Y. Kim, Sep. Sci. Technol. 35 (2000) 2327–2341.
- [7] S. Keysar, G.E. Shter, Y. de Hazan, Y. Cohen, G.S. Grader, Chem. Mater. 9 (1997) 2464–2467.
- [8] D. Mishra, S. Anand, R.K. Panda, R.P. Das, Mater. Lett. 42 (2000) 38–45.
- [9] J.J. Fitzgerald, G. Piedra, S.F. Dec, M. Seger, G.E. Maciel, J. Am. Chem. Soc. 119 (1997) 7832–7842.
- [10] L. Ji, J. Lin, K.L. Tan, H.C. Zeng, Chem. Mater. 12 (2000) 931–939.
- [11] D.J. Suh, T.J. Park, Chem. Mater. 9 (1997) 1903–1905.
- [12] S. Rezguit, B.C. Gates, Chem. Mater. 6 (1994) 2386–2389.
- [13] G. Paglia, C.E. Buckley, A.L. Rohl, R.D. Hart, K. Winter, A.J. Studer, B.A. Hunter, J.V. Hanna, Chem. Mater. 16 (2004) 220–236.
- [14] G. Paglia, C.E. Buckley, T.J. Udovic, A.L. Rohl, F. Jones, C.F. Maitland, J. Connolly, Chem. Mater. 16 (2004) 1914–1923.
- [15] T.F. Baumann, A.E. Gash, S.C. Chinn, A.M. Sawvel, R.S. Maxwell, J.H. Satcher, Chem. Mater. 17 (2005) 395–401.
- [16] G. Lefevre, M. Duc, P. Lepeut, R. Caplain, M. Fedoroff, Langmuir 18 (2002) 7530–7537.
- [17] M.L. Guzman-Castillo, X. Bokhimi, A. Toledo-Antonio, J. Salmones-Blasquez, F. Hernandez-Beltran, J. Phys. Chem. B 105 (2001) 2099–2106.
- [18] C.J. Harlan, M.R. Mason, A.R. Barron, Organometallics 13 (1994) 2957–2969.
- [19] H. Adkins, P. Perkins, J. Am. Chem. Soc. 47 (1925) 1163–1167.
- [20] H. Knözinger, Angew. Chem. Int. Ed. 7 (1968) 791–805.
- [21] H. Knözinger, R. Köhne, J. Catal. 5 (1966) 264–270.
- [22] H. Knözinger, H. Buhl, K. Kochloeff, J. Catal. 24 (1972) 57–68.
- [23] J.B. Peri, J. Phys. Chem. 69 (1965) 220–226.
- [24] H.A. Dabbagh, C.G. Hughes, B.H. Davis, J. Catal. 133 (1992) 445–460.
- [25] B. Shi, H.A. Dabbagh, B.H. Davis, J. Mol. Catal. A: Chem. 141 (1999) 257–262.
- [26] H.A. Dabbagh, J. Mohammad Salehi, J. Org. Chem. 63 (1998) 7619–7627.
- [27] H.A. Dabbagh, M.S. Yalfani, B.H. Davis, J. Mol. Catal. A: Chem. 238 (2005) 72–77.
- [28] E.J.W. Verway, Z. Kristallogr. 91 (1935) 65–69.
- [29] A. Ionescu, A. Allouche, J.P. Aycard, M. Rajzmann, F. Hutschka, J. Phys. Chem. B 106 (2002) 9359–9366.
- [30] O. Maresca, A. Allouche, J.P. Aycard, M. Rajzmann, S. Clemendot, F. Hutschka, J. Mol. Struct. Theochem. 505 (2000) 81–94.
- [31] G. Gutierrez, A. Taga, B. Johansson, Phys. Rev. B 65 (2002) 0121011–0121014.
- [32] T. Taniike, M. Tada, Y. Morikawa, T. Sasaki, Y. Iwasawa, J. Phys. Chem. B 110 (2006) 4929–4936.
- [33] K. Sohlberg, S.J. Pennycook, S.T. Pantelides, J. Am. Chem. Soc. 121 (1999) 7493–7499.
- [34] S. Cai, K. Sohlberg, J. Mol. Catal. A: Chem. 193 (2003) 157–164.
- [35] S. Cai, K. Sohlberg, J. Mol. Catal. A: Chem. 248 (2006) 76–83.
- [36] S. Cai, V. Chihai, K. Sohlberg, J. Mol. Catal. A: Chem. 275 (2007) 63–71.
- [37] C. Wolverton, K.C. Hass, Phys. Rev. B 63 (2000) 241021–2410216.
- [38] M. Digne, P. Sautet, P. Rayboud, P. Euzen, H. Toulhoat, J. Catal. 211 (2002) 1–5.
- [39] M. Digne, P. Sautet, P. Rayboud, P. Euzen, H. Toulhoat, J. Catal. 226 (2004) 54–68.
- [40] M.C. Valero, P. Rayboud, P. Sautet, J. Phys. Chem. B 110 (2006) 1759–1767.
- [41] M. Digne, P. Rayboud, P. Sautet, B. Rebours, H. Toulhoat, J. Phys. Chem. B 110 (2006) 20719–20720.
- [42] M. Sun, A.E. Nelson, J. Adjaye, J. Phys. Chem. B 110 (2006) 2310–2317.
- [43] A.E. Nelson, M. Sun, J. Adjaye, J. Phys. Chem. B 110 (2006) 20724–20726.
- [44] G. Paglia, C.E. Buckley, A.L. Rohl, B.A. Hunter, R.D. Hart, J.V. Hanna, L.T. Byrne, Phys. Rev. B 68 (2003) 1441101–14411011.
- [45] G. Paglia, C.E. Buckley, A.L. Rohl, J. Phys. Chem. B 110 (2006) 20721–20723.
- [46] L. Smrcok, V. Langer, J. Krestan, Acta Cryst. C62 (2006) i83–i84.
- [47] A.D. Becke, J. Chem. Phys. 104 (1996) 1040–1046.
- [48] C. Lee, W. Yang, R.G. Parr, Phys. Rev. B 37 (1988) 785–789.
- [49] M.J. Frisch, G.W. Trucks, H.B. Schlegel, G.E. Scuseria, M.A. Robb, J.R. Cheeseman, J.A. Montgomery, T. Vreven Jr., K.N. Kudin, J.C. Burant, J.M. Millam, S.S. Iyengar, J. Tomasi, V. Barone, B. Mennucci, M. Cossi, G. Scalmani, N. Rega, G.A. Petersson, H. Nakatsuji, M. Hada, M. Ehara, K. Toyota, R. Fukuda, J. Hasegawa, M. Ishida, T. Nakajima, Y. Honda, O. Kitao, H. Nakai, M. Klene, X. Li, J.E. Knox, H.P. Hratchian, J.B. Cross, C. Adamo, J. Jaramillo, R. Gomperts, R.E. Stratmann, O. Yazyev, A.J. Austin, R. Cammi, C. Pomelli, J.W. Ochterski, P.Y. Ayala, K. Morokuma, G.A. Voth, P. Salvador, J.J. Dannenberg, V.G. Zakrzewski, S. Dapprich, A.D. Daniels, M.C. Strain, O. Farkas, D.K. Malick, A.D. Rabuck, K. Raghavachari, J.B. Foresman, J.V. Ortiz, Q. Cui, A.G. Baboul, S. Clifford, J. Cioslowski, B.B. Stefanov, G. Liu, A. Liashenko, P. Piskorz, I. Komaromi, R.L. Martin, D.J. Fox, T. Keith, M.A. Al-Laham, C.Y. Peng, A. Nanayakkara, M. Challacombe, P.M.W. Gill, B. Johnson, W. Chen, M.W. Wong, C. Gonzalez, J.A. Pople, Gaussian 03, Revision B.02, Gaussian, Inc., Pittsburgh, PA, 2003.
- [50] B. Delley, J. Chem. Phys. 92 (1990) 508–517.
- [51] B. Delley, J. Chem. Phys. 113 (2000) 7756–7764.
- [52] E. Kim, P.F. Weck, S. Berber, D. Tománek, Phys. Rev. B 78 (2008) 1134041–1134044.
- [53] A. Ionescu, A. Allouche, J.P. Aycard, M. Rajzmann, R.L. Gall, J. Phys. Chem. B 107 (2003) 8490–8497.
- [54] G. Feng, C. Huo, C. Deng, L. Huang, Y. Li, J. Wang, H. Jiao, J. Mol. Catal. A: Chem. 304 (2009) 58–64.
- [55] H.S. Potdar, K.W. Jun, J.W. Bae, S.M. Kim, Y.J. Lee, Appl. Catal. A: Gen. 321 (2007) 109–116.
- [56] M.L. Guzman-Castillo, F. Hernandez-Beltran, J.J. Fripiat, A. Rodriguez-Hernandez, R. Garcia de Leon, J. Navarrete-Bolanos, A. Tobon-Cervantes, X. Bokhimi, Catal. Today 107 (2005) 874–878.
- [57] P. Alphonse, M. Courty, Thermochim. Acta 425 (2005) 75–89.
- [58] H.C. Lee, H.J. Kim, S.H. Chung, K.H. Lee, H.C. Lee, J.S. Lee, J. Am. Chem. Soc. 125 (2003) 2882–2883.
- [59] P.H. Colomban, J. Mater. Sci. Lett. 7 (1988) 1324–1326.
- [60] G. Urretavizcaya, A.L. Cavalieri, J.M. Porto Lopez, I. Sobrados, J. Sanz, J. Mater. Syn. Process. 6 (1998) 1–7.
- [61] X. Bokhimi, J.A. Toledo-Antonio, M.L. Guzman-Castillo, B. Mar-Mar, F. Hernandez-Beltran, J. Navarrete, J. Solid State Chem. 161 (2001) 319–326.
- [62] H.A. Dabbagh, K. Faghihi, Tetrahedron 56 (2000) 3611–3617.
- [63] D.A. De Vito, F. Gilardoni, L. Kiwi-Minsker, P.Y. Morgantini, S. Porchet, A. Renken, J. Weber, J. Mol. Struct. Theochem. 469 (1999) 7–14.
- [64] H. Aghabozorg, F. Manteghi, S. Sheshmani, J. Iran. Chem. Soc. 5 (2008) 184–227.